THE JOURNAL OF BIOLOGICAL CHEMISTRY VOL. 284, NO. 30, pp. 20147–20154, July 24, 2009

E_2P State Stabilization by the N-terminal Tail of the H,K-ATPase β-Subunit Is Critical for Efficient Proton Pumping under *in Vivo* Conditions*[S]

Received for publication, April 8, 2009, and in revised form, May 27, 2009 Published, JBC Papers in Press, June 2, 2009, DOI 10.1074/jbc.M109.005769

Katharina L. Dürr[‡1], Kazuhiro Abe[§], Neslihan N. Tavraz[‡], and Thomas Friedrich[‡]

From the [‡]Institute of Chemistry, Technical University of Berlin, Strasse des 17 Juni 135, D-10623 Berlin, Germany and the [§]Faculty of Sciences, Department of Biophysics, Kyoto University, Sakyo Ku, Kyoto 6068502, Japan

The catalytic α-subunits of Na,K- and H,K-ATPase require an accessory β-subunit for proper folding, maturation, and plasma membrane delivery but also for cation transport. To investigate the functional significance of the β-N terminus of the gastric H,K-ATPase *in vivo*, several N-terminally truncated β-variants were expressed in *Xenopus* oocytes, together with the S806C α-subunit variant. Upon labeling with the reporter fluorophore tetramethylrhodamine-6-maleimide, this construct can be used to determine the voltage-dependent distribution between E_1P/E_2P states. Whereas the E_1P/E_2P conformational equilibrium was unaffected for the shorter N-terminal deletions βΔ4 and βΔ8, we observed significant shifts toward E_1P for the two larger deletions βΔ13 and βΔ29. Moreover, the reduced $\Delta F/F$ ratios of βΔ13 and βΔ29 indicated an increased reverse reaction via $E_2P \rightarrow E_1P + ADP \rightarrow E_1 + ATP$, because cell surface expression was completely unaffected. This interpretation is supported by the reduced sensitivity of the mutants toward the E_2P-specific inhibitor SCH28080, which becomes especially apparent at high concentrations (100 μM). Despite unaltered apparent Rb^+ affinities, the maximal Rb^+ uptake of these mutants was also significantly lowered. Considering the two putative interaction sites between the β-N terminus and α-subunit revealed by the recent cryo-EM structure, the N-terminal tail of the H,K-ATPase β-subunit may stabilize the pump in the E_2P conformation, thereby increasing the efficiency of proton release against the million-fold proton gradient of the stomach lumen. Finally, we demonstrate that a similar truncation of the β-N terminus of the closely related Na,K-ATPase does not affect the E_1P/E_2P distribution or pump activity, indicating that the E_2P-stabilizing effect by the β-N terminus is apparently a unique property of the H,K-ATPase.

The gastric H,K-ATPase fulfills the remarkable task of pumping protons against a more than 10^6-fold concentration gradient. H^+ extrusion is coupled to countertransport of an equal number of K^+ ions for each ATP molecule hydrolyzed, resulting in an electroneutral overall process (1). Characteristic for all P-type ATPases, the enzyme cycles between the two principal conformational states (E_1 and E_2) and the corresponding phosphointermediates (E_1P and E_2P), which are formed by reversible phosphorylation of an aspartate residue in the highly conserved DKTGTLT motif. According to a Post-Albers-like reaction scheme (see Fig. 1*A*), the conformational $E_1P \rightarrow E_2P$ transition converts the high H^+/low K^+ affinity of the cation binding pocket into a low H^+/high K^+ affinity binding site, hence enabling proton release into the stomach lumen and subsequent binding of extracellular K^+. Because the pump faces a lumenal proton concentration of ~150 mM (2), proton release is probably the energetically most demanding step in the reaction cycle. Thus, during the conformational $E_1P \rightarrow E_2P$ transition, enormous pK_a changes of the H^+-coordinating residues have to occur that most likely involve the rearrangement of a positively charged lysine side chain (Lys-791 in rat H,K-ATPase) (3).

All P_2-type ATPases share a common catalytic α-subunit, composed of 10 transmembrane domains harboring the ion-binding sites and a large cytoplasmic loop with the nucleotide-binding domain, the phosphorylation domain (P-domain),[2] and the actuator domain (A-domain) (4). However, a unique feature of K^+-transporting Na,K- and H,K-ATPase enzymes is the requirement for an accessory β-subunit, which is indispensable for proper folding, maturation, and plasma membrane delivery (5, 6). Despite only 20–30% overall sequence identity between the H,K-ATPase β-subunit and the Na,K β-isoforms, the topogenic structure is similar: a short N-terminal cytoplasmic tail, followed by a single transmembrane segment and a large extracellular C-terminal domain with glycosylation sites and disulfide-bridging cysteines. Numerous studies have demonstrated that the β-subunit of the Na,K-ATPase is more than just a chaperone for the α-subunit, being also required for proper ion transport activity of the holoenzyme. In fact, it has been discovered that different cell- and tissue-specific β-isoforms have distinct effects on the cation affinities (7–9). Furthermore, it was shown that mutational changes in all three topogenic domains of the Na,K-ATPase β-subunit (10–19) as well as chemical

* This work was supported by Deutsche Forschungsgemeinschaft Grant SFB 740 and Cluster of Excellence "UNICAT" and Grants-in aid for Specially Promoted Research and by the Japan New Energy and Industrial Technology Development Organization.

[S] The on-line version of this article (available at http://www.jbc.org) contains supplemental Figs. S1 and S2 and additional references.

[1] To whom correspondence should be addressed: Institute of Chemistry, Technical University of Berlin, Secr. PC 14, Strasse des 17 Juni 135, D-10623 Berlin, Germany. Tel.: 49-30-314-24128; Fax: 49-30-314-78600; E-mail: katharina.duerr@TU-berlin.de.

[2] The abbreviations used are: P-domain, phosphorylation domain; TMRM, tetramethylrhodamine-6-maleimide; TM, transmembrane domain; EM, electron microscopy; WT, wild type; MES, 2-(*N*-morpholino)ethanesulfonic acid; MOPS, 3-(*N*-morpholino)-propanesulfonic acid; A-domain, actuator domain.

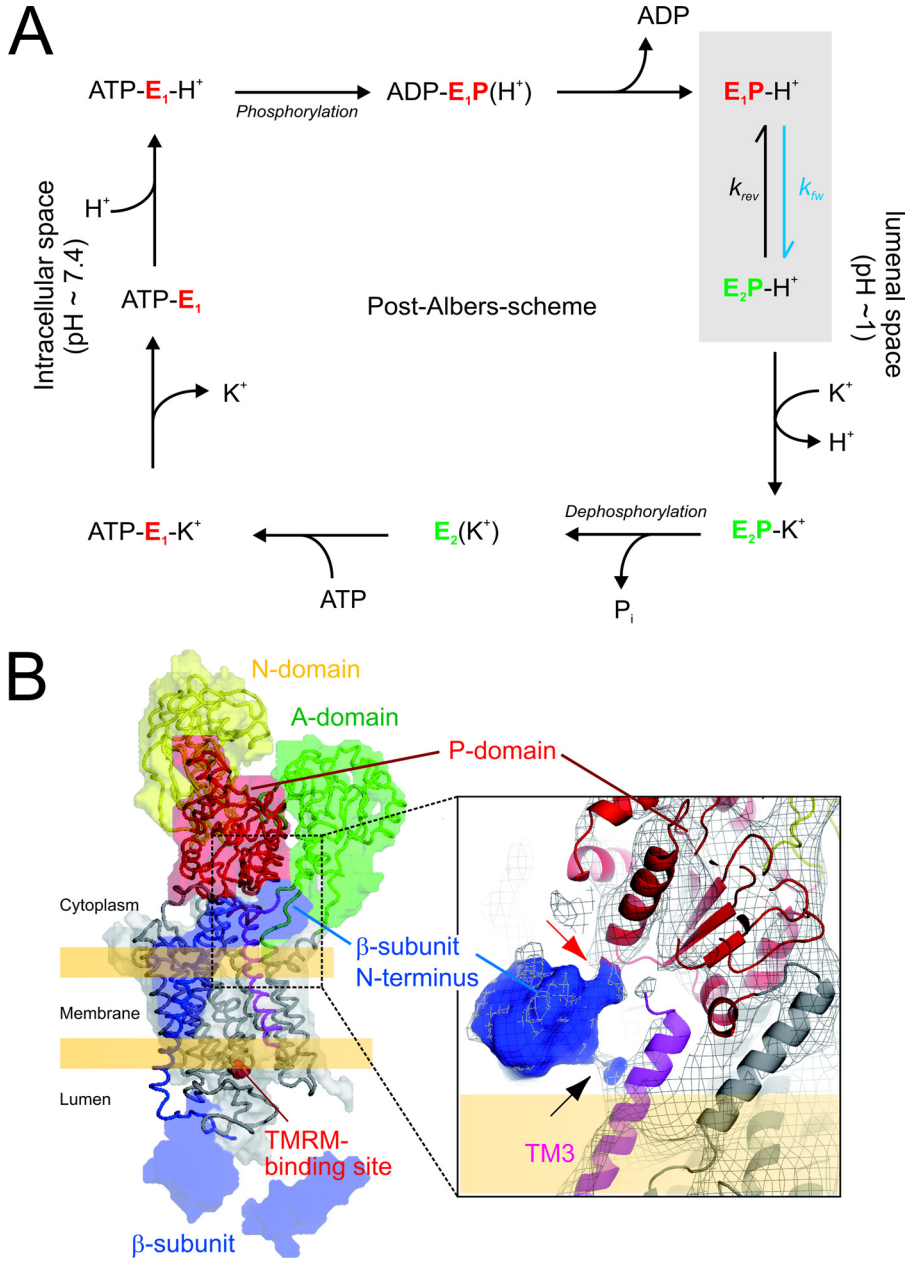

FIGURE 1. **Post-Albers scheme (*A*) and cryo-EM structural representation of pig gastric H,K-ATPase in the fluoroaluminate-bound pseudo-E_2P state (*B*).** *A*, Post-Albers scheme of the proposed reaction cycle of the gastric H,K-ATPase. E_1P/E_2P conformational states giving rise to voltage jump-induced fluorescence changes of TMRM-labeled H,K-ATPase molecules are highlighted (*gray box*). *B*, structural representation based on the cryo-EM structure of the pig gastric H,K-ATPase (surface or mesh, contoured at 1 σ; EM Data Bank code 5104) and the corresponding homology model (schematic; Protein Data Bank code 3IXZ). *Inset*, a close-up view (from the right side of the molecule) showing the putative interaction sites of the β-subunit N terminus with the P-domain (*red arrow*) and αTM3 (*black arrow*), respectively. Color coding is indicated in the figure.

interference with disulfide-forming cysteines in the Na,K-ATPase β-subunit ectodomain (20–22) affect the cation transport properties of the sodium pump. Finally, conformational changes in the β-subunit during the Na,K-ATPase reaction cycle were demonstrated by proteolytic digestion studies (23) and voltage clamp fluorometry (24).

Far less is known about the functional significance of the single H,K-ATPase β-isoform, especially about its potential impact on cation transport (reviewed in Refs. 25 and 26). We have proven recently that E_2P state-specific transmembrane interactions between residues in αTM7 and two highly conserved tyrosines in the βTM of both Na,K- and H,K-ATPase significantly stabilize the E_2P conformation (19). Mutational disruptions of this interaction resulted in substantial shifts toward E_1P and severely affected H^+ secretion, which highlighted the physiological relevance of this E_2P state stabilization. Notably, according to the recently published cryo-EM structure of pig gastric H,K-ATPase in the pseudo-E_2P state (27), the N-terminal tail of the β-subunit makes direct contact with the phosphorylation domain of the α-subunit (see Fig. 1*B*), thus indicating an additional E_2P state stabilization mediated by the β-N terminus. Although this idea was further supported by biochemical studies on N-terminally truncated mutants, direct evidence for this putative E_2P-stabilizing interaction and its potential significance for ion transport in intact cells is still lacking.

Here, we demonstrate for the first time the functional importance of the gastric H,K-ATPase β-subunit N terminus in living cells under *in vivo* conditions: voltage clamp fluorometry, Rb^+ flux, and SCH28080 sensitivity measurements revealed E_1P-shifted, ion transport-impaired phenotypes for two N-terminally truncated H,K β-variants, thus substantiating the E_2P-stabilizing effect of the β-N terminus suggested by the recent cryo-EM structure.

EXPERIMENTAL PROCEDURES

Molecular Biology and Oocyte Preparation—The cDNAs of the rat gastric H,K-ATPase β-subunit and a modified form of the α-subunit with a single cysteine replacement in the M5/M6 extracellular loop (S806C; Fig. 1*B*) were subcloned into vector pTLN (28). This cysteine replacement enables environmentally sensitive TMRM labeling of gastric H,K-ATPase (29) without affecting its transport properties (30). For Na,K-ATPase studies, an ouabain-insensitive sheep Na,K-ATPase α_1-mutant (carrying mutations Q111R and N122D (31)) without extracellularly exposed cysteines (mutations C911S and C964A (32)) and a Na,K-ATPase β_1-subunit variant (β_1S62C) that can be site-specifically labeled with TMRM (24) were used as templates for mutagenesis and cRNA preparation.

N-terminally truncated β-constructs were generated by recombinant PCR and verified by DNA sequencing. Oocyte preparation, cRNA synthesis, and injection were performed as described previously (30). Prior to experiments that were usually carried out 2 or 3 days after injection at 21–24 °C, the oocytes were preincubated in solutions containing 100 μM ouabain (Sigma-Aldrich) to inhibit the endogenous *Xenopus* Na,K-ATPase.

Voltage Clamp Fluorometry—Site-specific labeling of H,K (or Na,K)-ATPase-expressing oocytes was achieved by incubating oocytes in $HK_{7.4}$ buffer (90 mM NaCl, 20 mM tetraethylammonium chloride, 5 mM $BaCl_2$, 5 mM $NiCl_2$, 10 mM MOPS/Tris, pH 7.4) containing 5 μM TMRM (Molecular Probes) for 5 min at room temperature in the dark, followed by extensive washes in dye-free $HK_{7.4}$ buffer. Voltage clamp fluorometry measurements were carried out under high extracellular Na^+/K^+-free conditions for the characterization of H,K-ATPase mutants in $HK_{5.5}$ buffer (90 mM NaCl, 20 mM tetraethylammonium chloride, 5 mM $BaCl_2$, 5 mM $NiCl_2$, 10 mM MES/Tris, pH 5.5, 100 μM ouabain) and for Na,K-ATPase-expressing oocytes in $NaK_{7.4}$ buffer (100 mM NaCl, 5 mM $BaCl_2$, 5 mM $NiCl_2$, 10 mM Hepes, pH 7.4, 100 μM ouabain), respectively. Details on setup components, data acquisition, and analysis are given in Ref. 19.

Rb^+ Uptake Measurements—The oocytes were incubated for 15 min in Rb^+ flux buffer (5 mM RbCl, 85 mM tetramethylammonium chloride, 20 mM tetraethylammonium chloride, 5 mM $BaCl_2$, 5 mM $NiCl_2$, 10 mM MES, pH 5.5, 100 μM ouabain). After three washing steps in Rb^+-free washing buffer (90 mM tetramethylammonium chloride or NaCl, 20 mM tetraethylammonium chloride, 5 mM $BaCl_2$, 5 mM $NiCl_2$, 10 mM MES, pH 5.5) and one wash in water, each individual oocyte was homogenized in 1 ml of Millipore water. For SCH28080 inhibition experiments, the K^+-competitive inhibitor SCH28080 (Sigma-Aldrich) was added to the preincubation solution and Rb^+ flux buffer (to a final concentration of either 10 μM or 100 μM), respectively. To determine the apparent constant $K_{0.5}$ for half-maximal activation of the H,K-ATPase by rubidium, the sum [tetramethylammonium chloride] plus [RbCl] in the Rb^+ flux buffer was kept constant at 90 mM, *e.g.* 1 mM RbCl + 89 mM tetramethylammonium chloride. After subtraction of the average Rb^+ uptake into control oocytes from the same batches at a given [RbCl], the data were fitted to a Michaelis-Menten type function (Equation 1).

$$v = v_{max} \cdot \frac{[S]}{K_{0.5} + [S]} \quad \text{(Eq. 1)}$$

Aliquots of 20 μl from oocyte homogenates were analyzed by atomic absorption spectroscopy using an AAnalyst800™ spectrometer (PerkinElmer Life Sciences), equipped with a transversely heated graphite furnace using a temperature protocol according to the manufacturer's procedures (conditions available on request). Absorption was measured at 780 nm using a rubidium hollow cathode lamp (Photron, Melbourne, Australia). After Zeeman background correction, the Rb^+ contents were calculated by comparison with standard calibration curves (measured between 0 and 50 μg/liter Rb^+).

Western Blot Analysis of Isolated Plasma Membranes—The procedures for isolation of plasma membranes and total cellular membranes from *Xenopus* oocytes, gel electrophoresis, and immunoblotting were performed according to the protocols in Ref. 19. The polyclonal antibody HK12.18 (Merck) (6) and the monoclonal antibody 2B6 (MBL, Woburn, MA) (33) were used for detection of gastric H,K-ATPase α- and β-subunits, respectively.

RESULTS AND DISCUSSION

E_1P/E_2P Conformational Distribution of N-terminally Deleted H,K-ATPase β-Mutants—To investigate whether the N-terminal domain of the β-subunit indeed contributes to E_2P state stabilization of the gastric H,K-ATPase, we expressed the wild type β-subunit and four N-terminally deleted H,K β-mutants (Fig. 2*A*) together with the α-subunit variant S806C in *Xenopus* oocytes. After site-specific labeling of this cysteine with TMRM (Fig. 1*B*), monoexponential fluorescence changes were observed upon voltage jumps from a holding potential of −40 mV to values between −180 and +60 mV (Fig. 2*B*). Hence, this mutant α-subunit directly monitors the voltage-dependent distribution between the E_1P/E_2P states of H,K-ATPase enzymes, as demonstrated previously (19, 30). Fig. 2*C* shows the resulting voltage dependence of steady-state fluorescence amplitudes ($1 - \Delta F/F$), which follow a Boltzmann-type distribution for both wild type and β-N-terminally deleted H,K-ATPase enzymes. Whereas these curves were not changed for the shorter N-terminal deletions βΔ4 and βΔ8 compared with βWT, the distributions for the βΔ13 and βΔ29 truncated variants were significantly shifted toward more positive potentials (see Table 1 for Boltzmann parameters), indicating a relative destabilization of the E_2P state in favor of E_1P. According to these distributions, ~65% of the βWT and βΔ4- and βΔ8-containing H,K-ATPase molecules occur in the E_2P state at −60 mV (which is the physiologically relevant membrane potential determined for parietal cells (34)), but only 60 and 50% of the βΔ29 and βΔ13 mutant enzymes are present in E_2P, respectively. Furthermore, the E_1P shift is also reflected by the voltage-dependent reciprocal time constants obtained from monoexponential fits to the fluorescence changes (Fig. 2*D*); of note, these are significantly smaller for the βΔ29 and βΔ13 mutants than for the wild type only at positive potentials, which favor the forward reaction from E_1P to E_2P, but not at negative potentials, at which the enzyme is driven into the E_1P state (via the backward reaction described by k_{rev} in Figs. 1*A* and 2*D*). Therefore, these N-terminal deletions apparently cause a shift toward E_1P by reducing the "forward" rate constant (designated as k_{fw}) of the E_1P/E_2P transition without changing the rate constant k_{rev} for the "reverse" reaction.

However, if only the results shown in Fig. 2 (*C* and *D*) are considered, the conformational effect caused by the N-terminal deletions is probably underestimated because compared with βWT, the two variants βΔ13 and βΔ29 also showed substantially smaller values for the enzyme-specific fluorescence changes $\Delta F/F$ (Fig. 2*E*). Western blot analysis of isolated plasma membranes excluded the possibility that the lower $\Delta F/F$ values observed for the βΔ13 and βΔ29 constructs were simply due to a reduced cell surface delivery of the α-subunits that are avail-

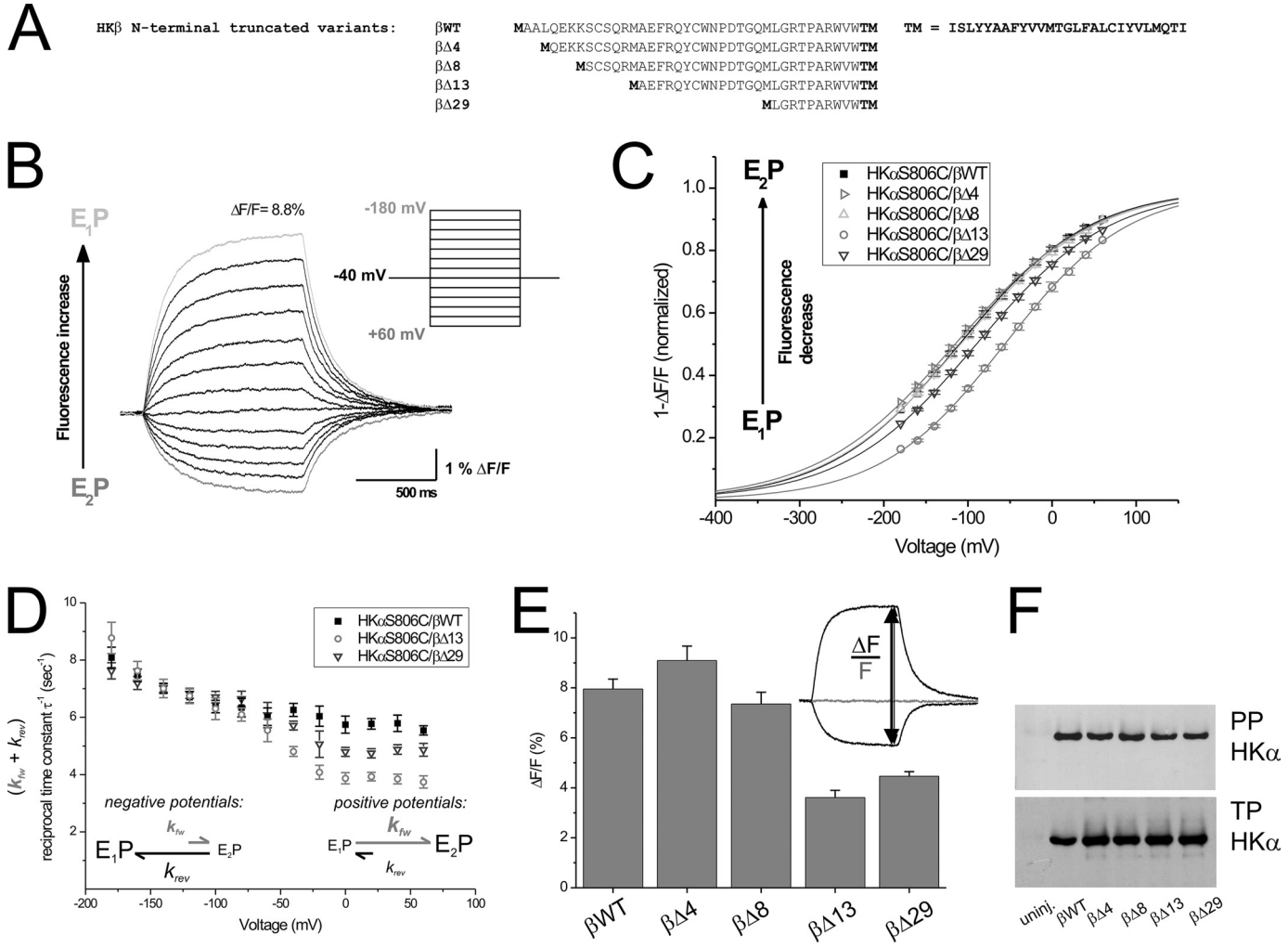

FIGURE 2. **Voltage-dependent E_1P/E_2P distribution and plasma membrane targeting of N-terminally deleted H,K-ATPase β-mutants.** *A*, partial amino acid sequence of N-terminally deleted H,K-ATPase β-variants and the wild type rat gastric H,K-ATPase β-subunit. *B*, voltage pulse-induced fluorescence signals of a TMRM-labeled oocyte expressing H,K-ATPase αS806C/βWT under high Na^+/K^+-free conditions at pH 5.5. *Inset*, voltage protocol. *C*, voltage-dependent distributions of fluorescence amplitudes $1 - \Delta F/F$ for H,K-ATPase complexes consisting of the α-subunit reporter construct αS806C and either unmodified HKβWT (■) or N-terminally deleted H,Kβ-variants βΔ4 (▷), βΔ8 (△), βΔ13 (○), and βΔ29 (▽). The data are the means ± S.E. of 15–30 oocytes from two or three different oocyte batches, normalized to saturating values obtained from fits of a Boltzmann function to the data (superimposed lines; see Table 1 for fit parameters). *D*, reciprocal time constants obtained by monoexponential fits of the voltage jump-induced fluorescence changes for wild type (■) and N-terminally deleted H,K-ATPase β-variants βΔ13 (○) and βΔ29 (▽). The data are the means ± S.E. of 10–16 oocytes. *E*, $\Delta F/F$ values (in %) for TMRM-labeled oocytes expressing αS806C and either the wild type H,K-ATPase β-subunit or N-terminally truncated β-variants. The data are the means ± S.E. of 13–32 oocytes from three different oocyte batches. *Inset*, $\Delta F/F$ is calculated from the difference ΔF (represented by a *black arrow*) between the fluorescence at the most hyperpolarizing voltage (−180 mV, *upper black trace*) and the most depolarizing voltage (+60 mV, *lower black trace*), normalized to the background fluorescence F at −40 mV (*gray trace*). *F*, Western blot analysis of plasma membrane (*PP*, *upper panel*) and total membrane (*TP*, *lower panel*) preparations from H,K-ATPase-expressing oocytes, using anti-H,Kα antibody HK12.18 or anti-H,Kβ antibody 2B6 (see supplemental Fig. S1). The equivalent of two oocytes was loaded per lane; detection of the endogenous *Xenopus* Na,K-ATPase α_1-isoform served as a loading standard, which is shown in supplemental Fig. S1.

TABLE 1

Parameters from fits of a Boltzmann function to $(1 - \Delta F/F)/V$ distributions of N-terminally deleted H,K-ATPase β-mutants (Fig. 2*C*)

The values are the means ± S.E. of 15–30 oocytes from two or three different oocyte batches.

	Boltzmann parameter $(1 - \Delta F/F)/V$ curves	
	$V_{0.5}$	z_q
	mV	
HKαS806C/βWT	−110.1 ± 5.0	0.33 ± 0.01
HKαS806C/βΔ4	−115.3 ± 5.8	0.31 ± 0.01
HKαS806C/βΔ8	−108.7 ± 4.3	0.32 ± 0.02
HKαS806C/βΔ13	−56.3 ± 6.3	0.34 ± 0.02
HKαS806C/βΔ29	−89.9 ± 4.3	0.32 ± 0.01

able for labeling with TMRM (Fig. 2*F* and supplemental Fig. S1). Therefore, it is safe to assume that the shown $\Delta F/F$ ratio is directly proportional to the number of H,K-ATPase molecules that can be shifted between E_1P/E_2P states by voltage jumps (according to the reaction sequence highlighted in *gray* in Fig. 1*A*). The ~2-fold lower $\Delta F/F$ values observed for the βΔ13 and βΔ29 mutants (compared with βWT, βΔ4, and βΔ8) most likely reflect a higher tendency of the mutant H,K-ATPase molecules (that accumulate in the E_1P state because of the reduced k_{fw}) to undergo further backward reactions via $E_1P\ (H^+) \rightarrow E_1P + H^+ + ADP \rightarrow E_1 + H^+ + ATP$. The resulting substantial depletion in the sum of E_1P/E_2P states would therefore explain the observed smaller fluorescence changes. This interpretation is

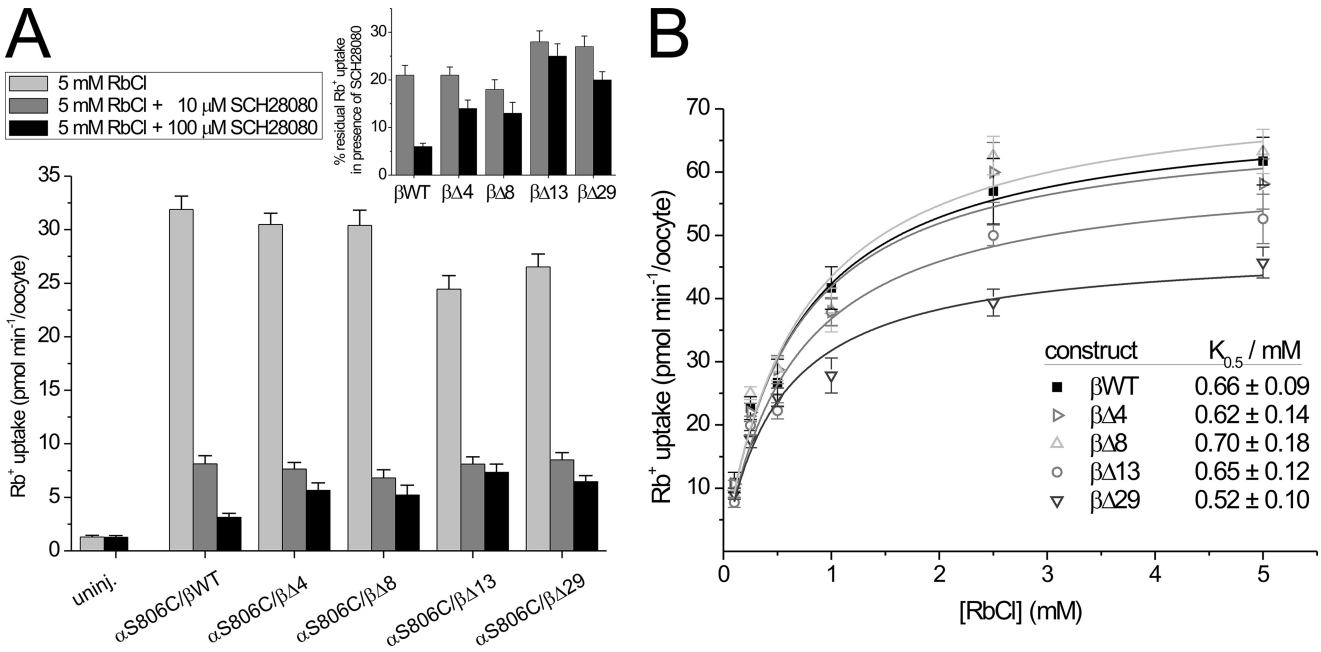

FIGURE 3. **Rb^+ uptake, SCH28080 sensitivity and apparent Rb^+ affinity of N-terminally truncated H,K-ATPase variants.** *A*, Rb^+ uptake was determined at pH 5.5 in extracellular Na^+-free solutions containing 5 mM RbCl in the absence (*light gray bars*) or presence of SCH28080 (*dark gray bars*, 10 μM; *black bars*, 100 μM). *Inset*, residual Rb^+ uptake activity (in %) in the presence of 10 μM (*dark gray bars*) or 100 μM (*black bars*) SCH28080. The data were normalized to Rb^+ uptake at 5 mM RbCl in the absence of SCH28080 for each construct after subtraction of the mean Rb^+ uptake of uninjected oocytes. The data are the means ± S.E., n = 40–50 oocytes from three or four independent experiments. *B*, Michaelis-Menten plots are shown for concentration-dependent Rb^+ uptake by H,K-ATPase-expressing oocytes. The oocytes were injected with cRNAs of the αS806C mutant and either the wild type β-subunit (■) or N-terminally deleted β-variants βΔ4 (▷), βΔ8 (△), βΔ13 (○), and βΔ29 (▽) cRNA, respectively. The data are the means ± S.E., n = 10–20 oocytes. One representative of at least two independent experiments is shown. Apparent half-maximal activation constants $K_{0.5}$ (Table 2) were obtained from a fit of a Michaelis-Menten type function to the data (*superimposed lines*).

actually in line with previous results from pulse-chase experiments on purified membranes of H,K-ATPase-expressing HEK293 cells. Compared with the wild type, the membrane fractions containing β-N-terminally truncated variant βΔ8, βΔ13 (27), or βΔ28[3] showed increased reactivity of radiolabeled $E_1{}^{32}P$-phosphoenzymes with ADP to form [γ-^{32}P]ATP via the aforementioned reverse reaction. Of note, in these chase experiments, already the βΔ8 mutant exhibited a significantly reduced amount of ^{32}P-phosphoenzyme after a 5-s chase with ADP. However, care has to be taken when comparing these and our voltage clamp fluorometry results because of the differences in experimental conditions. The pulse-chase experiments have been performed on membrane fractions at a ubiquitous pH of 6.4, lower ionic strength, and 0 °C, whereas voltage clamp fluorometry probes the enzyme within an intact membrane environment with physiological ion concentrations (and neutral intracellular pH) at room temperature. Differences in the intracellular ion concentration or pH may well affect intramolecular interactions, especially if these interactions involve potentially charged residues (amino acids 6–8 in the N-terminal sequence MAALQEKKSC…). Furthermore, the intracellular ATP and Mg^{2+} concentrations are by far higher in *Xenopus* oocytes than in the pulse-chase experiments (2.3 mM ATP (35), 0.5 mM Mg^{2+} *versus* 10 μM ATP, 20 μM Mg^{2+}), thus favoring the forward phosphorylation reaction. Therefore, small effects on the E_1P/E_2P distribution that would reflect enhanced ADP-dependent dephosphorylation of the E_1P state of the βΔ8 mutant are possibly obscured under the conditions in living cells.

TABLE 2

Rb^+ uptake activity, SCH28080 sensitivity, and apparent Rb^+ affinity of N-terminally deleted H,K-ATPase β-mutants (see Fig. 3)

	Normalized Rb^+ uptake activity (5 mM RbCl)[a,b]	Residual Rb^+ uptake activity in presence of SCH28080[a,c]		Apparent Rb^+ affinity ($K_{0.5}$)[d]
		10 μM SCH28080	100 μM SCH28080	
	%	%		mM
HKαS806C/βWT	100 ± 3.9	21 ± 2.0	6 ± 0.7	0.66 ± 0.09
HKαS806C/βΔ4	96 ± 3.3	21 ± 1.7	14 ± 1.8	0.62 ± 0.14
HKαS806C/βΔ8	95 ± 4.4	18 ± 2.0	13 ± 2.3	0.70 ± 0.18
HKαS806C/βΔ13	77 ± 4.0	28 ± 2.3	25 ± 2.6	0.65 ± 0.12
HKαS806C/βΔ29	83 ± 3.8	27 ± 2.2	20 ± 1.7	0.52 ± 0.10
Uninjected	4 ± 0.4			

[a] The values are the means ± S.E. of 40–50 oocytes from three or four different oocyte batches.
[b] The data were normalized to Rb^+ uptake of HKαS806C/βWT, corresponding to 32 pmol/min/oocyte.
[c] The data were normalized to Rb^+ uptake at 5 mM RbCl in the absence of SCH28080 for each construct after subtraction of the mean Rb^+ uptake of uninjected oocytes.
[d] The values are the means ± S.E. of 10–20 oocytes.

Rb^+ Uptake and SCH28080 Sensitivity of N-terminally Truncated H,K-ATPase β-Subunits—To assess the impact on ion transport activity potentially caused by the conformational shifts of the N-terminally truncated β-variants, we determined Rb^+ uptake at saturating extracellular concentrations. Whereas Rb^+ uptake for βΔ4- and βΔ8-expressing oocytes was comparable with βWT, it was ~20% lower for βΔ13 and βΔ29 (Fig. 3*A* and Table 2). This can be interpreted as a reduced turnover number (lowered v_{max}) because the apparent affinity for extracellular Rb^+ was unaffected by the trunca-

[3] K. Abe, unpublished results.

tions (see Fig. 3*B* and Table 2 for apparent $K_{0.5}$ values). The affected turnover numbers of the βΔ13 and βΔ29 mutants demonstrate that obviously the transition that is characterized by the reduced rate constant k_{fw} of these variants directly affects the rate-limiting step of the catalytic cycle. This illustrates how already small shifts in conformational equilibria can have significant functional consequences for the transport activity of the gastric H,K-ATPase.

In the presence of 10 μM SCH28080, an E_2P-specific inhibitor of the H,K-ATPase (36–38), the Rb^+ uptake of βWT-, βΔ4-, and βΔ8-expressing oocytes was reduced to ~20% (Fig. 3*A*, *inset*, and Table 2), in agreement with the data of Mathews *et al.* (39). In contrast, the inhibition of ATPase complexes containing βΔ13 and βΔ29 was less efficient, resulting in significantly higher residual activities of ~30% at 10 μM SCH28080. Notably, 100 μM SCH28080 resulted in a suppression of Rb^+ uptake to ~6% residual activity for HKαS806C/βWT, whereas the effect was much smaller for any of the N-terminally deleted β-variants. As a possible consequence of the E_1P-shifted phenotypes of the mutants, the mean dwell time of molecules in the SCH28080-sensitive E_2P state may be substantially shorter. Thus, increasing the inhibitor concentration would not result in enhanced binding of the compound because the dwell time in E_2P is not sufficient to reach binding equilibrium under turnover conditions. In contrast, the wild type H,K-ATPase, which stays longer in E_2P, is able to bind more inhibitor molecules if the SCH28080 concentration is increased. Interestingly, at the higher inhibitor concentration, a significantly reduced SCH28080 sensitivity was also observed for βΔ4- and βΔ8-expressing oocytes, which showed a more than 2-fold higher residual activity compared with βWT (13–14% *versus* 6%). This suggests that already the shorter deletions cause an elevated preference for E_1P, which raises the question of why no effect on the conformational distribution (Fig. 2*C*) was seen for these constructs. Two possibilities may account for this: (i) minute shifts in the voltage-dependent E_1P/E_2P distribution may be difficult to resolve by voltage clamp fluorometry experiments because low slope factors z_q of the Boltzmann curves limit the accuracy of $V_{0.5}$ determination, and (ii) E_2-destabilizing effects that act on the relative distribution of pump molecules over all reaction intermediates may not be effective during the partial reaction sequence studied in pre-steady-state experiments (voltage clamp fluorometry) but rather become apparent under steady-state conditions (Rb^+ uptake), in which the enzyme undergoes the full reaction cycle.

Although the reduction in Rb^+ transport activity of βΔ13 and βΔ29 truncated mutants appears moderate, it is important to note that these subtle effects were observed already at a relatively mild proton gradient ($pH_{int} \sim 7.4$ *versus* $pH_{ext} = 5.5$). However, *in vivo* the H,K-ATPase pumps protons against a 10,000-fold higher gradient of ~10^6. Under these physiological conditions (which are unfortunately not applicable to *Xenopus* oocytes), the high lumenal H^+ concentration would even more favor H^+ reverse binding at the extracellular sites, thereby also stimulating the $E_2P \rightarrow E_1P$ "backward" reaction (*i.e.* increasing k_{rev}). An enhanced k_{rev} in addition to the reduced forward rate constant k_{fw} (as observed for the N-terminally deleted mutants βΔ13 and βΔ29) is thus expected to have even more drastic effects on the turnover number. Therefore, although causing only small effects at the rather shallow pH gradient applied here, the E_2P state destabilization by the β-N-terminal truncations will almost certainly slow down H^+ secretion under the pH conditions in the stomach.

A surprising finding from the current study is that the more extensive deletion βΔ29 caused a smaller shift toward the E_1P state than βΔ13 (Fig. 2*C* and Table 1). The two putative interaction sites between the β-N terminus and the α-subunit proposed by the recently published cryo-EM structure of the pig gastric H,K-ATPase (27) may provide a rationale to explain these rather unexpected effects; apart from the aforementioned contact between the β-N terminus and the P-domain (probably near Arg-716 to Ala-719; see *red arrow* in Fig. 1*B*), a stretch of the β-N terminus located closer to the transmembrane domain also approaches the cytoplasmic stalk of αTM3, which is connected to the A-domain (Fig. 1*B*, *black arrow*). Therefore, truncation of the first 12 amino acids in βΔ13 may only disrupt the interaction with the P-domain and thereby cause the strong E_1P shift, whereas the more extensive deletion in βΔ29 most likely affects both critical contacts, which might involve an additional compensatory mechanism (see below).

As outlined by Abe *et al.* (27), the contact between the β-subunit N terminus and the P-domain probably stabilizes the enzyme in E_2P, thereby minimizing the reverse reaction with ADP via $E_2P \rightarrow E_1P + ADP \rightarrow E_1 + ATP$ in terms of a "ratchet"-like mechanism. In the pseudo-E_2P state revealed by the cryo-EM structure, the nucleotide-binding domain of the α-subunit is retracted far from the P-domain (supplemental Fig. S2). Therefore, reverse transfer of the phosphate (bound to Asp-385 in the P-domain) to ADP (bound to the nucleotide-binding domain) would require a large movement of the P-domain, which is presumably prohibited by the tethering between the P-domain and β-N terminus in the E_2 state. In contrast, in a putative E_1P state derived from a SERCA-E_1AlF_4-ADP structure (40), the ADP at the nucleotide-binding domain is in close proximity to the phosphate analogue AlF_4^- (shown in supplemental Fig. S2), which could thus explain the enhanced ADP rephosphorylation of the E_1P-shifted N-terminally deleted β-variants (27).

The interaction of the β-N terminus with the A-domain via the movement of αTM3 may also be functionally significant because the protrusion of the TGES loop from the A-domain into the gap between the N- and P-domains may have a segregating effect, too (supplemental Fig. S2). Although the influence of the β-N/αTM3 contact on positioning of the A-domain is not resolved yet, it seems possible that the missing contact to the β-N terminus via αTM3 (in βΔ29) may lead to unrestricted movement of the A-domain. This may promote the segregating effect of the TGES loop, which could partially compensate for the destabilization of E_2P that arises from the missing interaction with the P-domain, thus explaining the less E_1P-shifted phenotype of βΔ29 compared with βΔ13.

N-terminal Truncation of the Na,K-ATPase β-Subunit—Notably, according to the recently published crystal structure of the closely related Na,K-ATPase in the Rb^+-occluded E_2 state (41), there is no indication for similar interactions between the β-N terminus and the α-subunit of the sodium pump. Although

A

```
HKβWT     MAALQEKKSCSQRMAEFRQYCWNPDTGQMLGRTPARWVWTM
HKβΔ4       MQEKKSCSQRMAEFRQYCWNPDTGQMLGRTPARWVWTM
HKβΔ8         MSCSQRMAEFRQYCWNPDTGQMLGRTPARWVWTM
HKβΔ13          MAEFRQYCWNPDTGQMLGRTPARWVWTM
HKβΔ29                  MLGRTPARWVWTM
NaKβ1WT     MARGKAKEEGSWKKFIWNSEKKEFLGRTGGSWFKTM
NaKβ1Δ8       MEGSWKKFIWNSEKKEFLGRTGGSWFKTM

TM = transmembrane domain
```

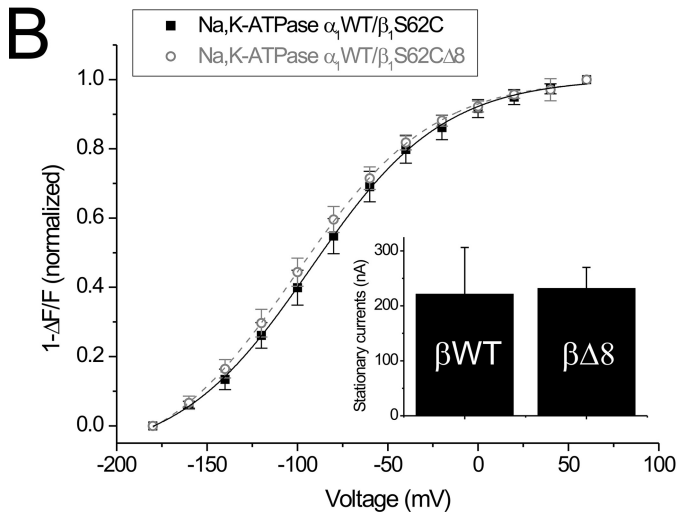

FIGURE 4. **Conformational E_1P/E_2P distribution and pump currents of β-N-terminally truncated Na,K-ATPase.** *A*, partial amino acid sequences of the N-terminally deleted Na,K-ATPase β-variant NaKβ$_1$Δ8 and the wild type sheep Na,K-ATPase β$_1$-subunit (in *black*). For comparison, the wild type and N-terminally truncated β-variants of the rat H,K-ATPase are also shown (in *gray*). *B*, voltage-dependent distribution of fluorescence amplitudes $1 - \Delta F/F$ for Na,K-ATPase complexes consisting of the sheep wild type α$_1$-subunit and either the unmodified reporter construct β$_1$S62C (■) or the N-terminally deleted Na,K β-variant β$_1$S62CΔ8 (○). The same voltage protocol as in Fig. 2 (*B–D*) was applied in 100 mM Na^+/K^+-free solution at pH 7.4. The data are the means ± S.D. of 10–15 oocytes, normalized to saturating values at −180 mV after subtracting the values for −60 mV. A curve corresponding to the fit of a Boltzmann function is superimposed, and the resulting fit parameters $V_{0.5}$ and z_q are listed in Table 3. *Inset*, stationary pump currents of the two constructs at saturating K^+ concentrations (10 mM). The data are the means ± S.D. of 10–15 oocytes.

TABLE 3

Stationary pump currents and parameters from fits of a Boltzmann function to $(1 - \Delta F/F)/V$ distributions of β-N-terminally truncated Na,K-ATPase (Fig. 4)

The values are the means ± S.D. of 10–15 oocytes.

	Boltzmann parameter $(1 - \Delta F/F)/V$ curves		Stationary pump currents at 10 mM KCl
	$V_{0.5}$	z_q	
	mV		*nA*
NaKα$_1$WT/β$_1$S62C	−92.7 ± 7.7	0.70 ± 0.03	221 ± 85
NaKα$_1$WT/β$_1$S62CΔ8	−100.8 ± 7.5	0.68 ± 0.03	232 ± 38

the β-N terminus of the Na,K-ATPase was not completely resolved in this structure so that evidence for a similar interaction in the Na,K-ATPase is absent so far, we tried to explore whether the intersubunit interaction mediated by the H,K-ATPase β-N terminus is conserved among P_{2C}-type ATPases. To determine the impact of β-N-terminal truncation on sheep Na,K-ATPase, the eight most N-terminal amino acids of reporter construct β$_1$S62C (24) of the β$_1$-subunit were deleted (Fig. 4*A*). Because the cytoplasmic β-N terminus of the Na,K-ATPase is shorter than that of the gastric H,K-ATPase, this truncation results in a N-terminal domain comparable in length to the βΔ13 variant of the H,K-ATPase. This N-terminally truncated β-variant, NaKβ$_1$S62CΔ8, was coexpressed with the wild type sheep α$_1$-subunit, labeled by TMRM, and subjected to voltage jumps in a K^+-free solution containing 100 mM Na^+. The resulting voltage-dependent distribution of fluorescence amplitudes is not significantly different from the one observed for full-length β$_1$S62C-containing Na,K-ATPase complexes (Fig. 4*B* and Table 3). Furthermore, as inferred from the stationary pump currents at 10 mM K^+, the ion transport activity of the Na,K-ATPase is completely unaffected by the β-N-terminal truncation (Fig. 4*B*, *inset*). Regarding the comparably shallow Na^+ gradient under physiological conditions, an analogous ratchet-like E_2P stabilization is probably not necessary to assist Na^+ transport of the sodium pump. This further supports our hypothesis that the E_2P state stabilization mediated by the H,K-ATPase β-N terminus is unique to facilitate proton transport against the steep proton gradient across the parietal cell membrane, which is ~10,000-fold higher than the typical transmembrane gradient for Na^+ ions. Therefore, the mechanism of E_2P state stabilization by the gastric H,K-ATPase β-N terminus appears to be a distinctive property of this enzyme.

Conclusions—As a key observation, the recently published cryo-EM structure of the gastric H,K-ATPase highlighted the close proximity between the P-domain of the α-subunit and the short N-terminal tail of the β-subunit, suggesting an E_2P-stabilizing interaction of the two subunits. The current study on N-terminally truncated β-variants provides direct evidence that the β-N terminus assists in E_2P state stabilization and that this is critical for the transport efficiency of the enzyme under *in vivo* conditions. Because the effects of the mutants were already significant under the relatively shallow H^+ gradient (ΔpH ≈2), they may even be more relevant for the enzyme *in situ*, where a strong E_2P preference is essential for efficient H^+ release against a ΔpH of ~6 units. Moreover, because we recently demonstrated an E_2P-stabilizing effect of interactions between residues in the transmembrane domain of the H,K-ATPase β-subunit and TM7 of the α-subunit, the two effects exerted by different regions of the β-subunit may synergistically contribute to the functional requirement of E_2P state stabilization.

Acknowledgments—We thank I. Seuffert for excellent technical assistance, Ernst Bamberg for continuous encouragement, and K. Tani for valuable comments.

REFERENCES

1. Sachs, G., Chang, H. H., Rabon, E., Schackman, R., Lewin, M., and Saccomani, G. (1976) *J. Biol. Chem.* **251,** 7690–7698
2. Wallmark, B., Lorentzon, P., and Sachs, G. (1990) *J. Intern. Med. Suppl.* **732,** 3–8
3. Sachs, G., Shin, J. M., Vagin, O., Lambrecht, N., Yakubov, I., and Munson, K. (2007) *J. Clin. Gastroenterol.* **41,** S226–S242
4. Toyoshima, C., Nakasako, M., Nomura, H., and Ogawa, H. (2000) *Nature* **405,** 647–655

5. McDonough, A. A., Geering, K., and Farley, R. A. (1990) *FASEB J.* **4,** 1598–1605
6. Gottardi, C. J., and Caplan, M. J. (1993) *J. Biol. Chem.* **268,** 14342–14347
7. Jaisser, F., Jaunin, P., Geering, K., Rossier, B. C., and Horisberger, J. D. (1994) *J. Gen. Physiol.* **103,** 605–623
8. Blanco, G., and Mercer, R. W. (1998) *Am. J. Physiol. Renal Physiol.* **275,** F633–F650
9. Crambert, G., Hasler, U., Beggah, A. T., Yu, C., Modyanov, N. N., Horisberger, J. D., Lelièvre, L., and Geering, K. (2000) *J. Biol. Chem.* **275,** 1976–1986
10. Jaunin, P., Jaisser, F., Beggah, A. T., Takeyasu, K., Mangeat, P., Rossier, B. C., Horisberger, J. D., and Geering, K. (1993) *J. Cell Biol.* **123,** 1751–1759
11. Eakle, K. A., Kabalin, M. A., Wang, S. G., and Farley, R. A. (1994) *J. Biol. Chem.* **269,** 6550–6557
12. Noguchi, S., Mutoh, Y., and Kawamura, M. (1994) *FEBS Lett.* **341,** 233–238
13. Geering, K., Beggah, A., Good, P., Girardet, S., Roy, S., Schaer, D., and Jaunin, P. (1996) *J. Cell Biol.* **133,** 1193–1204
14. Hasler, U., Crambert, G., Horisberger, J. D., and Geering, K. (2001) *J. Biol. Chem.* **276,** 16356–16364
15. Hasler, U., Wang, X., Crambert, G., Béguin, P., Jaisser, F., Horisberger, J. D., and Geering, K. (1998) *J. Biol. Chem.* **273,** 30826–30835
16. Abriel, H., Hasler, U., Geering, K., and Horisberger, J. D. (1999) *Biochim. Biophys. Acta* **1418,** 85–96
17. Shainskaya, A., and Karlish, S. J. (1996) *J. Biol. Chem.* **271,** 10309–10316
18. Shainskaya, A., Schneeberger, A., Apell, H. J., and Karlish, S. J. (2000) *J. Biol. Chem.* **275,** 2019–2028
19. Dürr, K. L., Tavraz, N. N., Dempski, R. E., Bamberg, E., and Friedrich, T. (2009) *J. Biol. Chem.* **284,** 3842–3854
20. Lutsenko, S., and Kaplan, J. H. (1993) *Biochemistry* **32,** 6737–6743
21. Kirley, T. L. (1990) *J. Biol. Chem.* **265,** 4227–4232
22. Kawamura, M., Ohmizo, K., Morohashi, M., and Nagano, K. (1985) *Biochim. Biophys. Acta* **821,** 115–120
23. Lutsenko, S., and Kaplan, J. H. (1994) *J. Biol. Chem.* **269,** 4555–4564
24. Dempski, R. E., Friedrich, T., and Bamberg, E. (2005) *J. Gen. Physiol.* **125,** 505–520
25. Geering, K. (2001) *J. Bioenerg. Biomembr.* **33,** 425–438
26. Chow, D. C., and Forte, J. G. (1995) *J. Exp. Biol.* **198,** 1–17
27. Abe, K., Tani, K., Nishizawa, T., and Fujiyoshi, Y. (2009) *EMBO J.* **28,** 1637–1643
28. Lorenz, C., Pusch, M., and Jentsch, T. J. (1996) *Proc. Natl. Acad. Sci. U.S.A.* **93,** 13362–13366
29. Geibel, S., Zimmermann, D., Zifarelli, G., Becker, A., Koenderink, J. B., Hu, Y. K., Kaplan, J. H., Friedrich, T., and Bamberg, E. (2003) *Ann. N.Y. Acad. Sci.* **986,** 31–38
30. Dürr, K. L., Tavraz, N. N., Zimmermann, D., Bamberg, E., and Friedrich, T. (2008) *Biochemistry* **47,** 4288–4297
31. Price, E. M., and Lingrel, J. B. (1988) *Biochemistry* **27,** 8400–8408
32. Hu, Y. K., Eisses, J. F., and Kaplan, J. H. (2000) *J. Biol. Chem.* **275,** 30734–30739
33. Mori, Y., Fukuma, K., Adachi, Y., Shigeta, K., Kannagi, R., Tanaka, H., Sakai, M., Kuribayashi, K., Uchino, H., and Masuda, T. (1989) *Gastroenterology* **97,** 364–375
34. Demarest, J. R., and Machen, T. E. (1985) *Am. J. Physiol. Cell Physiol.* **249,** C535–C540
35. Gribble, F. M., Loussouarn, G., Tucker, S. J., Zhao, C., Nichols, C. G., and Ashcroft, F. M. (2000) *J. Biol. Chem.* **275,** 30046–30049
36. Wallmark, B., Sachs, G., Mardh, S., and Fellenius, E. (1983) *Biochim. Biophys. Acta* **728,** 31–38
37. Mendlein, J., and Sachs, G. (1990) *J. Biol. Chem.* **265,** 5030–5036
38. Keeling, D. J., Taylor, A. G., and Schudt, C. (1989) *J. Biol. Chem.* **264,** 5545–5551
39. Mathews, P. M., Claeys, D., Jaisser, F., Geering, K., Horisberger, J. D., Kraehenbuhl, J. P., and Rossier, B. C. (1995) *Am. J. Physiol. Cell Physiol.* **268,** C1207–C1214
40. Toyoshima, C., Nomura, H., and Tsuda, T. (2004) *Nature* **432,** 361–368
41. Morth, J. P., Pedersen, B. P., Toustrup-Jensen, M. S., Sørensen, T. L., Petersen, J., Andersen, J. P., Vilsen, B., and Nissen, P. (2007) *Nature* **450,** 1043–1049